CHAPTER IV

RESEARCH METHODOLOGY

4.1 Overview

To fulfill the objectives of this thesis, the author decided to perform the tests at seven locations located in Bangkok, Kanchanaburi, and Chiang Mai. The specific addresses of the sites are as follows;

a. Chulalongkorn University (CU), Bangkok, Thailand 10330. Coordinates: Latitude 13°44 17.87 N/ Longitude 100°31 52.06 E
b. Meteorological Department of Thailand (TMD), Bangna, Bangkok, Thailand. Coordinates: Latitude 13°40 6.7 N/ Longitude 100°36 24.4 E
c. Asian Institute of Technology (AIT), Pathumthani, Thailand. Coordinates: Latitude 14°04 50.1 N/ Longitude 100°36 39.9 E
d. KirdKao Observatory, Kanchanaburi, Thailand. Coordinates: Latitude 14°28 51.5 N/ Longitude 99°26 44.3 E
e. Meteorological Station of Kanchanaburi (TMD), Thailand. Coordinates: Latitude 14°01 19.8 N/ Longitude 99°32 9 E
f. Chiang Mai University, Chiang Mai, Thailand. Coordinates: Latitude 18°47 38.7 N/ Longitude 98°57 7.8 E
g. Wat Chedi Luang, Chiang Mai, Thailand. Coordinates: Latitude 18°47 14.6 N/ Longitude 98°59 11.9 E

The sites (a, b, and c) are in Bangkok and assumed to have similar soil condition, while (d, e) and (f, g) are located in the western and the northern of Thailand, respectively.

The way to obtain the shear wave velocity profile from MASWM typically consists of three successive steps:

1. Data acquisition: the process to obtain the raw data in term of arrival time and space from the series of field measurement.

2. Data Processing: the raw data is transformed to f-k domain by the Two Dimensional Fast Fourier Transform (2DFFT). The locus of peak in f-k spectrum is used to construct the dispersion curve (Rayleigh phase velocity vs. Frequency).
3. Data inversion: the shear wave velocity vs. depth is attained from this step. In surface wave method, $\lambda/3$ *or* $\lambda/2$ approaches are considered as the simplified algorithm for data inversion, which is adapted in this thesis. It assumes that the vertical shear wave velocity approximately equals to 110% of the Rayleigh wave phase velocity and the associated depth is equivalent to one-third or one-half of the wavelength.

4.2 Research Framework

The overall framework of this research is summarized in the flow chart below (Figure 4.1).

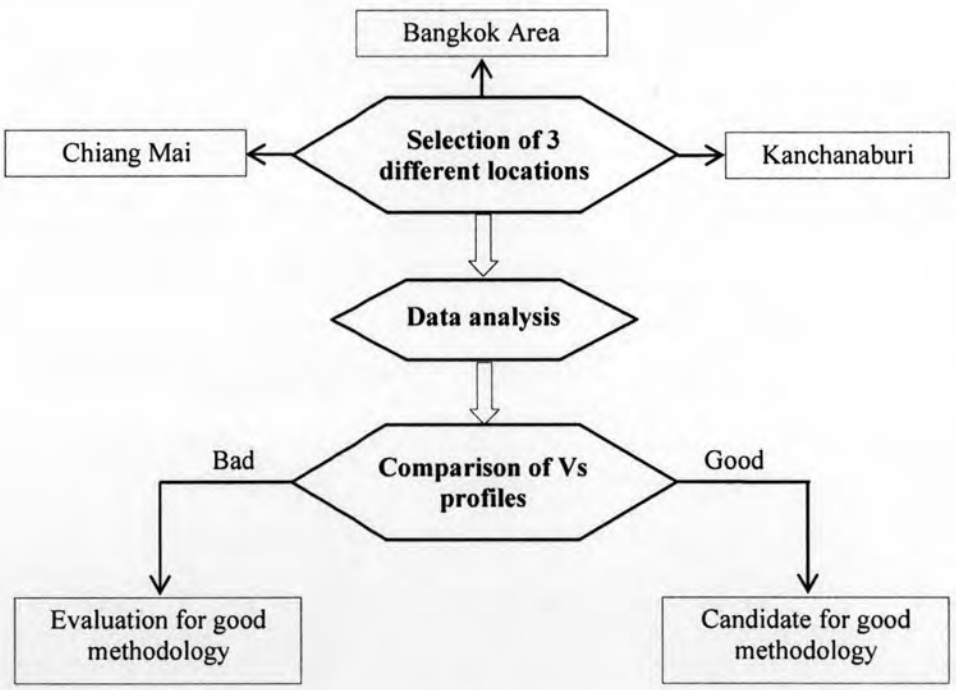

Figure 4-1 Flow chart of research framework

It is shown to guide a sequence of tasks which begins with the data collection from various sites mentioned in section 4.1. The geological condition of those seven places is expected to be different which is good for the validation of MASWM. After the

field measurement has been analyzed, obtained velocity profiles, then, are compared with those from seismic downhole test, boring report and SCPT. As long as good agreements are achieved, the final conclusion can be drawn directly. On the contrary, if the mismatch is noticed, the evaluation for good methodology will be done.

4.3 Research Assumption

- Only a fundamental mode of wave propagation is taken into account in data inversion process
- Wavelengths collected from the experiment are apparent wavelengths which are determined by the geometric arrangement of geophones.
- In view of the fact that we use the simplified inversion algorithm, the Poisson's ratio is assumed to be about 0.25 so that ratio between V_R and V_S equal to 0.911.

4.4 Data Collection

For data collection, the test setup is the most significant part. It is adjusted according to many criteria and the limit number of the equipment.

4.4.1 Field Equipment

Three necessary parts of the equipment consist of seismic source for generating incident waves, receivers for detecting the signal from the source, and seismograph for recording the time history captured by receivers. The equipment in this research is in small scale to facilitate transportation and human power purposes. The seismic source is a 10 lb sledge hammer with a $(18 \times 18 \times 1.5)\ cm$ plate steel (figure 4-2). The seismograph is a 24 channels acquisition board (NR-2000, figure 4-3). Sixteen low natural frequency geophones (HS-1-LT 2Hz-3810Ω) (figure 4-4a), are deployed because of their sensitivity and ability to detect the long waves (with low frequencies). The geophones have the sensitivity of 2 volt/inch/second and coil resistance of 3810 ohms specified at 25°C. The seismic response between output and frequency is shown in figure 4-5.

Figure 4-2 **A 10 lb sledge hammer and a plate steel used as seismic source**

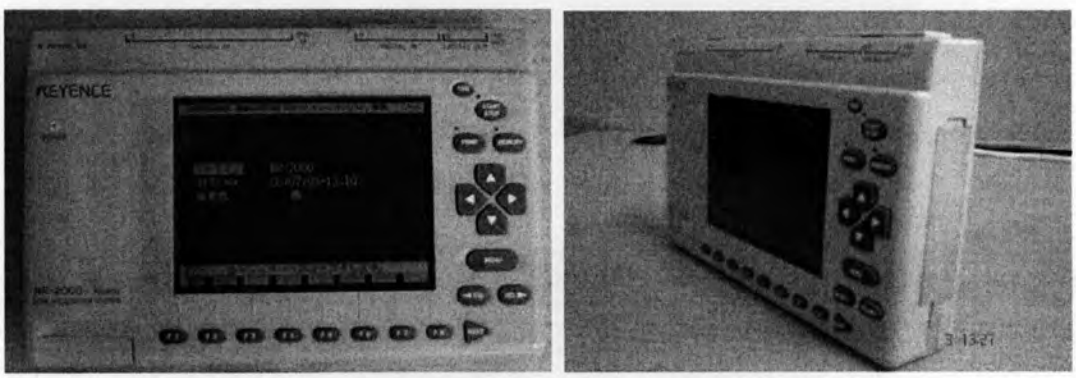

Figure 4-3 **Data acquisition board, NR-2000**

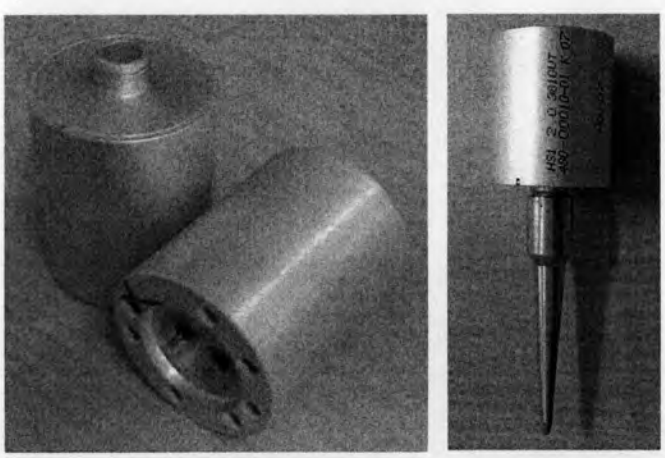

Figure 4-4 **(a) Low frequency geophone (HS-1-LT 2.0Hz-3810Ω) (b) geophone attached with 9cm spike**

A 2 Hz seismometer is usually large and heavy, but in this case it is quite compact with 5.08 cm in height, 4.12 cm in diameter, and 247 g in weight (figure 4.3a). For

good coupling with the ground, the 9cm spikes are attached to the bottom of geophones (Figure 4.4b).

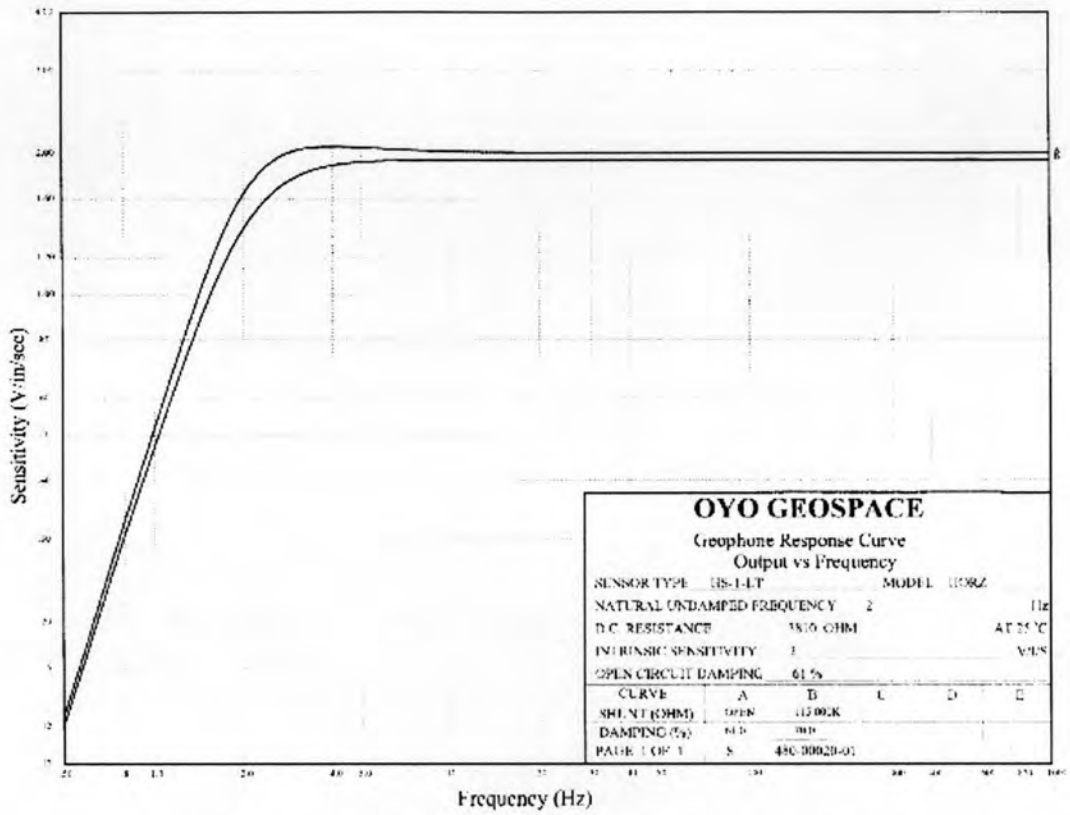

Figure 4-5 Seismic detector response curve output vs. Frequency

4.4.2 Test Setup

Before setting up the test many factors have to be taken into account such as the number and natural frequency of geophone, source-receiver configuration, and energy of seismic source. These field parameters strongly affect the resolution and quality of the data. In this study, the test configurations at seven sites are summarized in the table 4-1 and Figure 4-6.

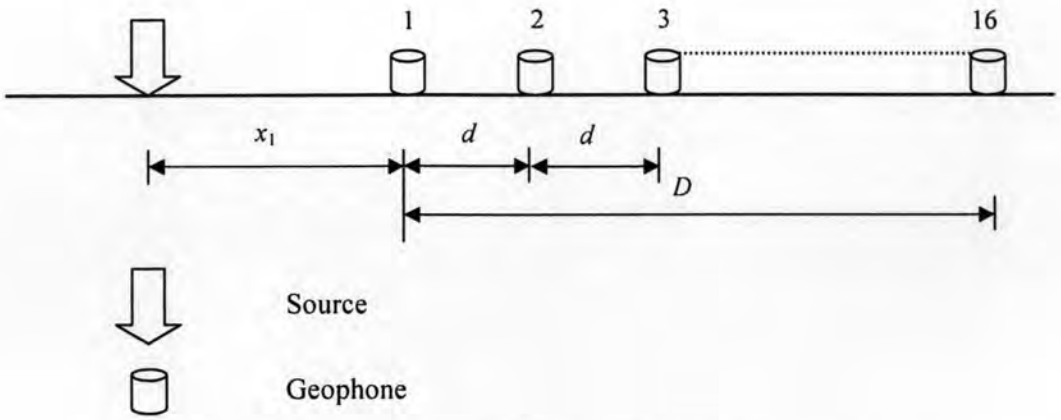

Figure 4-6 Scheme of field setup for data acquisition

Table 4-1 Active Source Acquisition Parameters

Acquisition parameters	**a**	**b**	**c**	**d**	**e**	**f**	**g**	Unit
x_1	9	6	9	5	8	6	6	m
d	4	2	3	1	2	2	2	m
D	60	30	45	15	30	30	30	m
Sampling rate	1	1	1	1	1	1	1	ms
Record length	1.6	1	1.6	1	1	1.6	1	s

Note: the letter (a, b, c, d, e, f, and g) represent the sites as mentioned in section 4.1

To achieve the target depth of investigation around 30m the spreads longer than 30m were used (according to SeisImager/SW Manual, 2005 and the simplified inversion algorithm). From SeisImager/SW Manual (2005), the minimum measurable wavelength is defined by two times of the smallest geophone spacing and the maximum measurable wavelength is equal to the largest geophone interval. This can be implied from inversion algorithm ($\lambda/3 \ \ or \ \ \lambda/2$)(mention in section 4.6) that if the spread length is 30m, the estimated depth of investigation is equal to one half or one third the total spread length corresponding to 20m or 30m, respectively. Nevertheless, the test configuration for each test is varied according to the limitation of space in field and the source energy. In the case of site (**a**) performed on football field at Chulalongkorn University, we were able to extend the spread length up to 60m. For the locations (**b**, **e**, **f**, and **g**), the spaces were enough for only 30m array and the

distance from the source (hammer and plate steel) to the first geophone of 6 to 8m. For the site at AIT (**c**), a low energy source was able to reach the farthest geophone in the range of 45m. Unlike the other fields, the site (**d**) is located on the mountain where the underlying layer below 4 m is bed rock. Therefore, downhole and boring results are not available. For this site, the MASW test was performed to acquire the shear wave velocity around 15m depth.

As for the signal processing, the sampling frequency was set to 1 kHz for all tests. The recording times vary from 1s to 1.6s, which allow us to record the full wave form travelling through the sixteen geophones. By Nyquist theory as mentioned before, the highest usable frequency is equal to 500Hz (or one-half of 1000 Hz). This limit should be adequate for geotechnical applications.

4.4.3 Raw Data

To improve the signal to noise ratio, stacking technique was applied by taking the average of recorded signals from 8 to 10 events. After stacking, the seismic data are graphically shown from figure 4-7 to 4-13 successively while the whole data sets are written in attached CD.

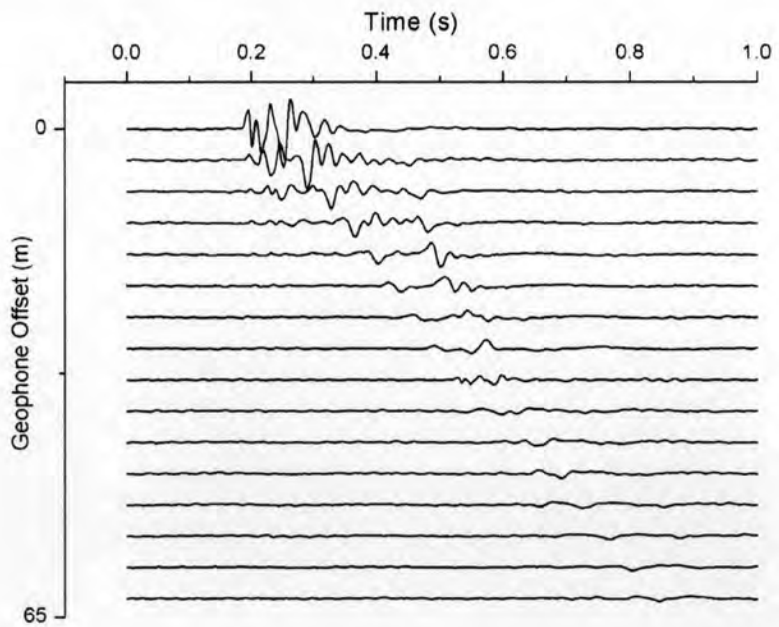

Figure 4-7 Seismic data in the space-time domain with geophone interval 4m and record time 1.6s gathered at Chulalongkorn University.

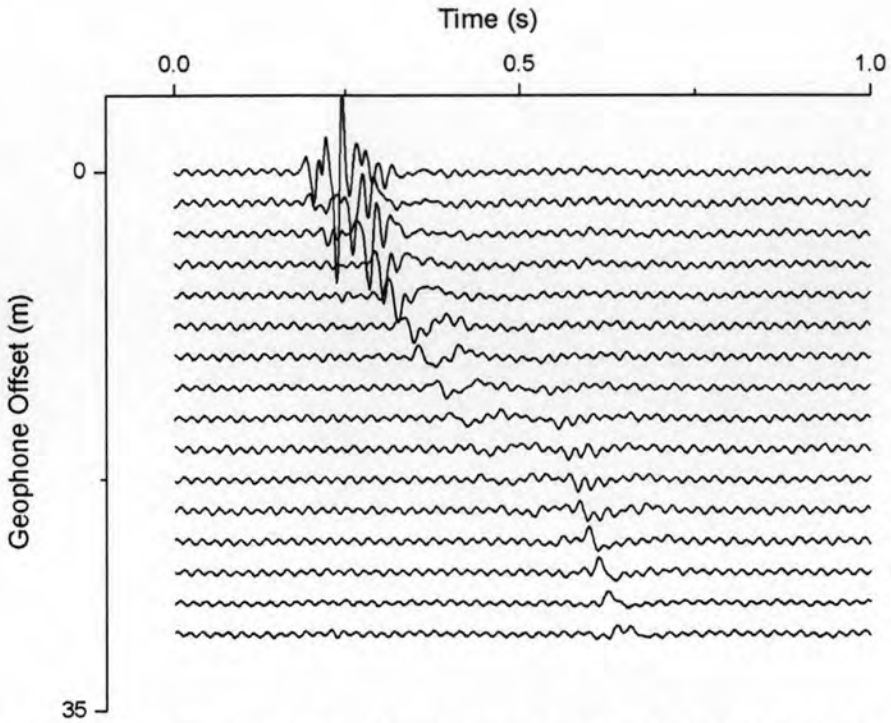

Figure 4-8 **Seismic data in the space-time domain with geophone interval 2m and record time 1s gathered at TMD, Bangkok.**

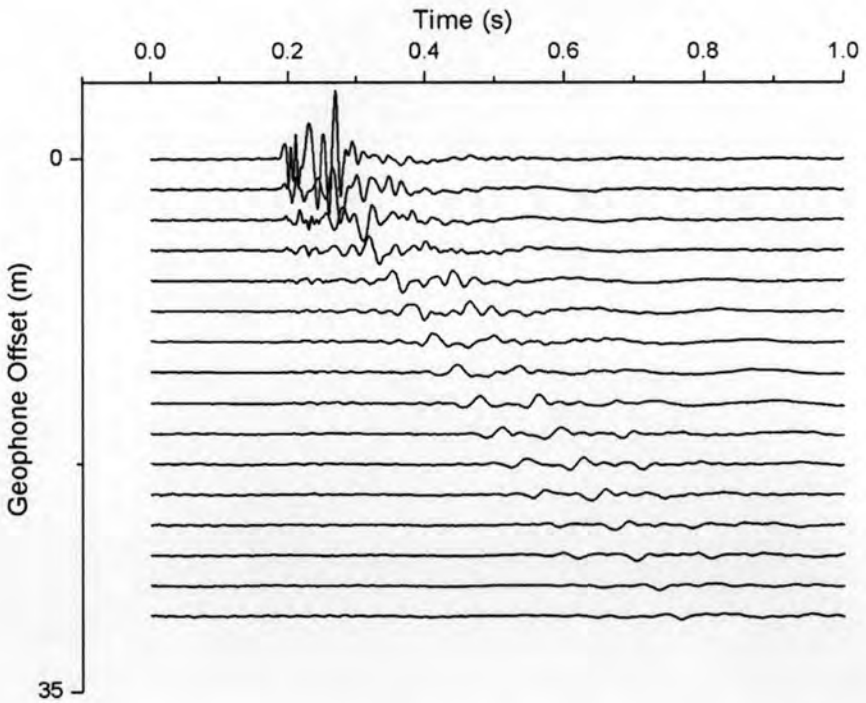

Figure 4-9 **Seismic data in the space-time domain with geophone interval 2m and record time 1.6s gathered at AIT.**

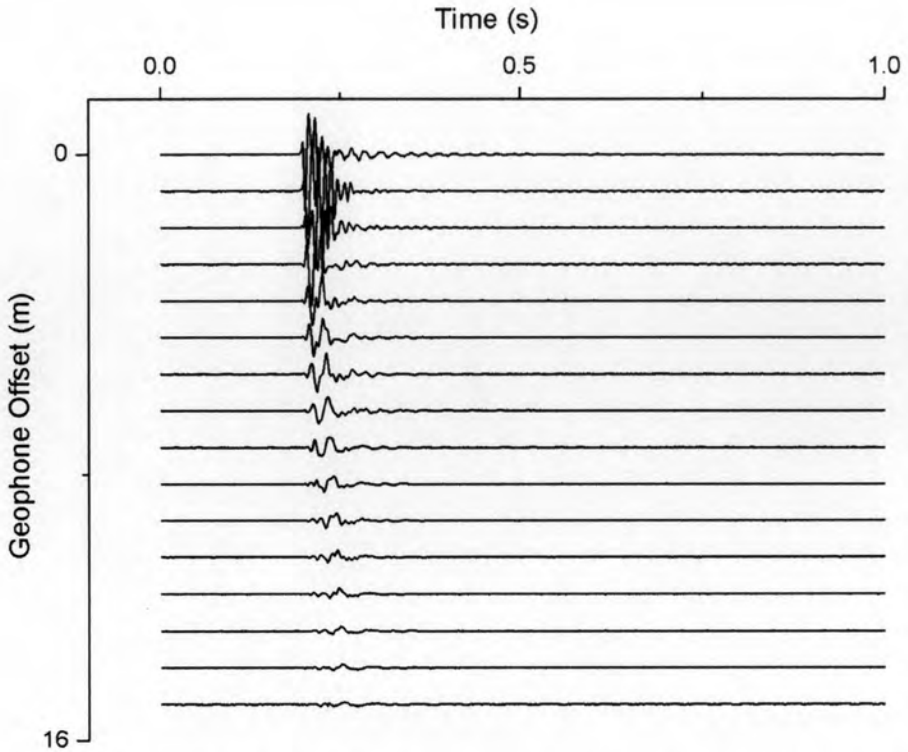

Figure 4-10 **Seismic data in the space-time domain with geophone interval 1m and record time 1s gathered at Kirdkao Observatory, Kanchanaburi.**

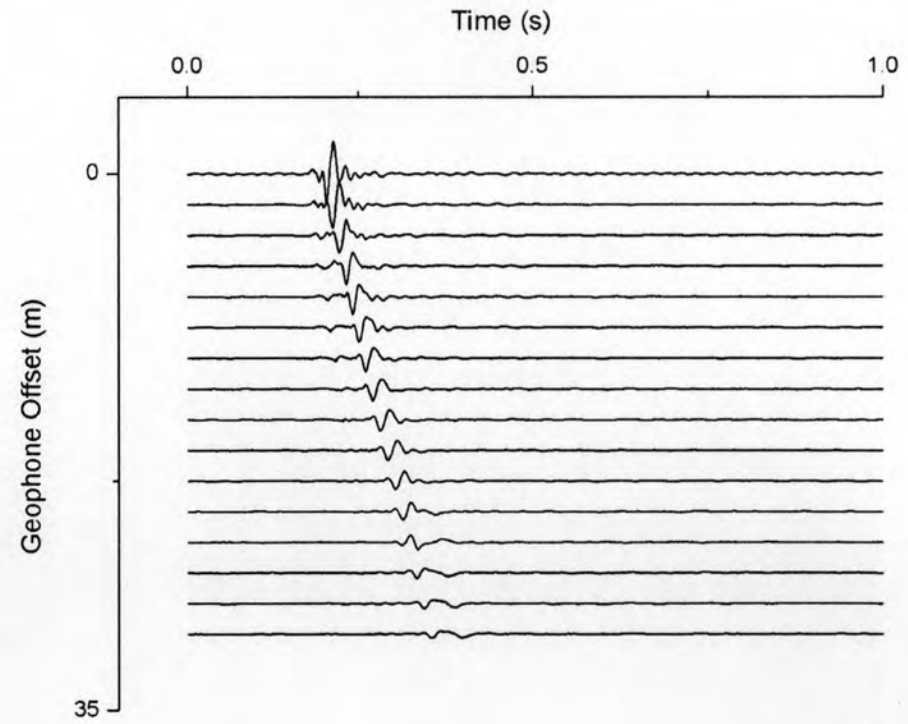

Figure 4-11 **Seismic data in the space-time domain with geophone interval 2m and record time 1s gathered at TMD, Kanchanaburi.**

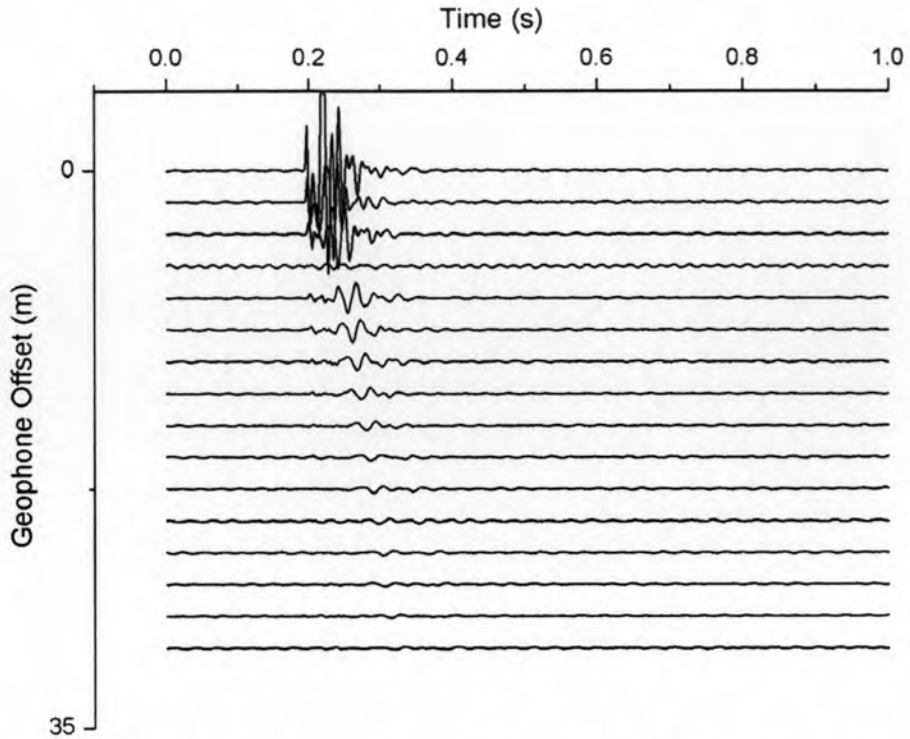

Figure 4-12 **Seismic data in the space-time domain with geophone interval 2m and record time 1.6s gathered at Chiang Mai University.**

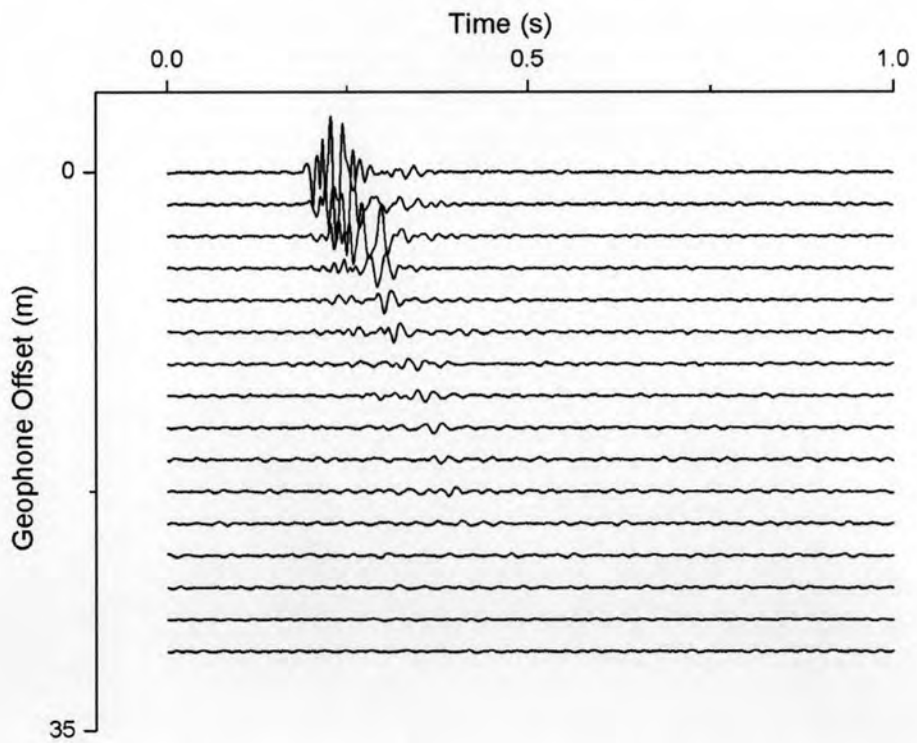

Figure 4-13 **Seismic data in the space-time domain with geophone interval 2m and record time 1s gathered at Wat Chediluang, Chiang Mai.**

In point of fact, primary judgment can be made from the space-time domain plots whether the perturbations are able to reach the target depth of investigation or not by first looking at the number of channel that detect the signal. Subsequently, notice the distance between the first geophone to that channel, it will approximately inform the exploration depth after signal processing phase. The magnitude of amplitude in each trace of geophones is also reflected a quality of the data. The higher amplitude recorded in the first few geophones comparing to the distance ones might give bad effects on data analysis. Among all the sites, the raw data at TMD Kanchanburi shows a better proportion of amplitude at sixteen geophones for which the test configuration at this site was different from the others with x_1 = 8m and D = 30m.

4.5 Data Processing

In data processing, 2D FFT is a convenient method to filter out the unwanted noise from the useful signal. However, it is not possible to compute by hand. The discrete raw data in term of arrival time and geophone spacing are quite a big number which needed the computer software to perform calculations. To do that, the raw data are converted into matrix form (attached CD) with input dimensions according to field parameters. The columns are defined according to geophone coordinate while the rows are time coordinate. After transformation, the higher energy of the Rayleigh waves appears in the f-k plot with red color surrounded by yellow one in a long thread, which is easily distinguished from the ambient noise as shown in figure 4-14 to 4-20.

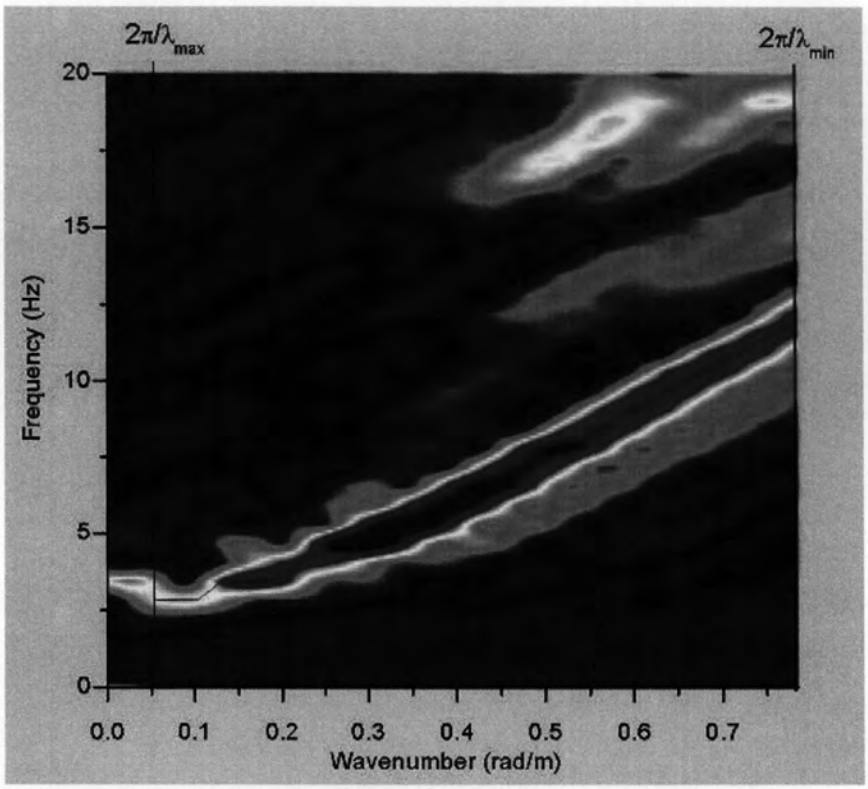

Figure 4-14 **Frequency wavenumber domain for Chulalongkorn University**

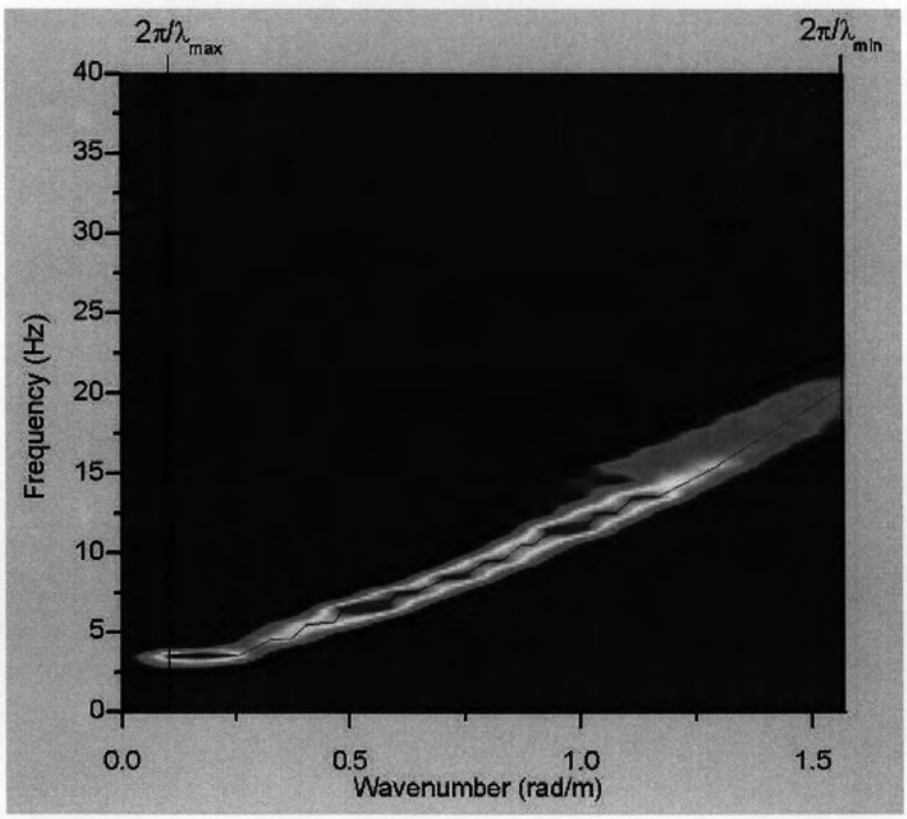

Figure 4-15 **Frequency wavenumber domain for TMD, Bangkok**

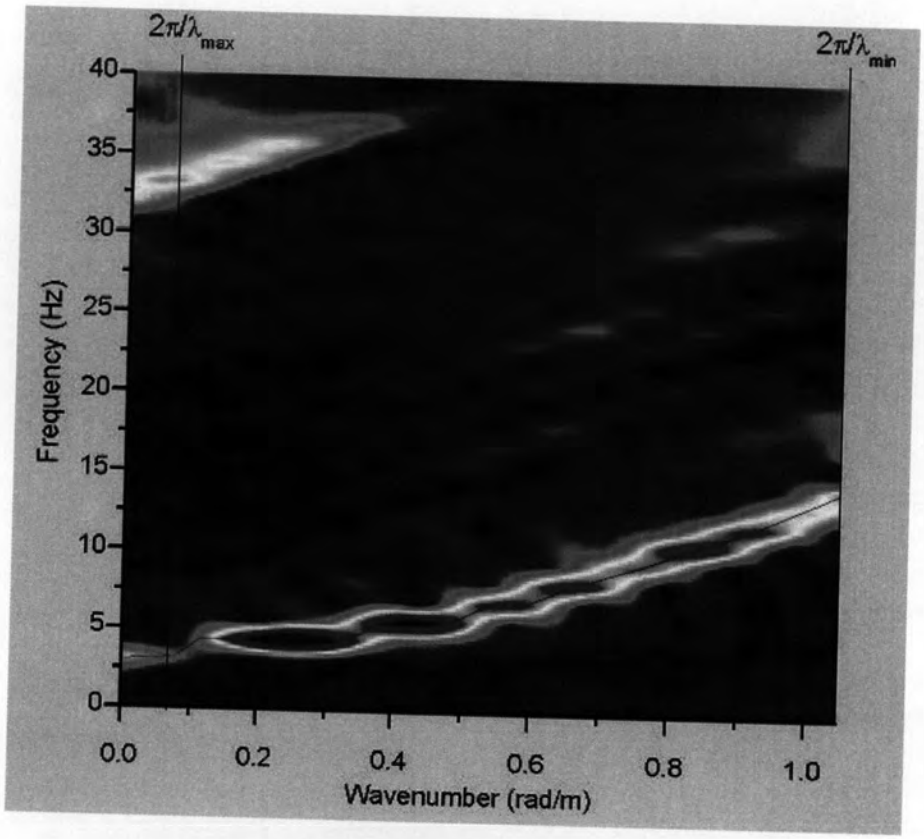

Figure 4-16 **Frequency wavenumber domain for AIT**

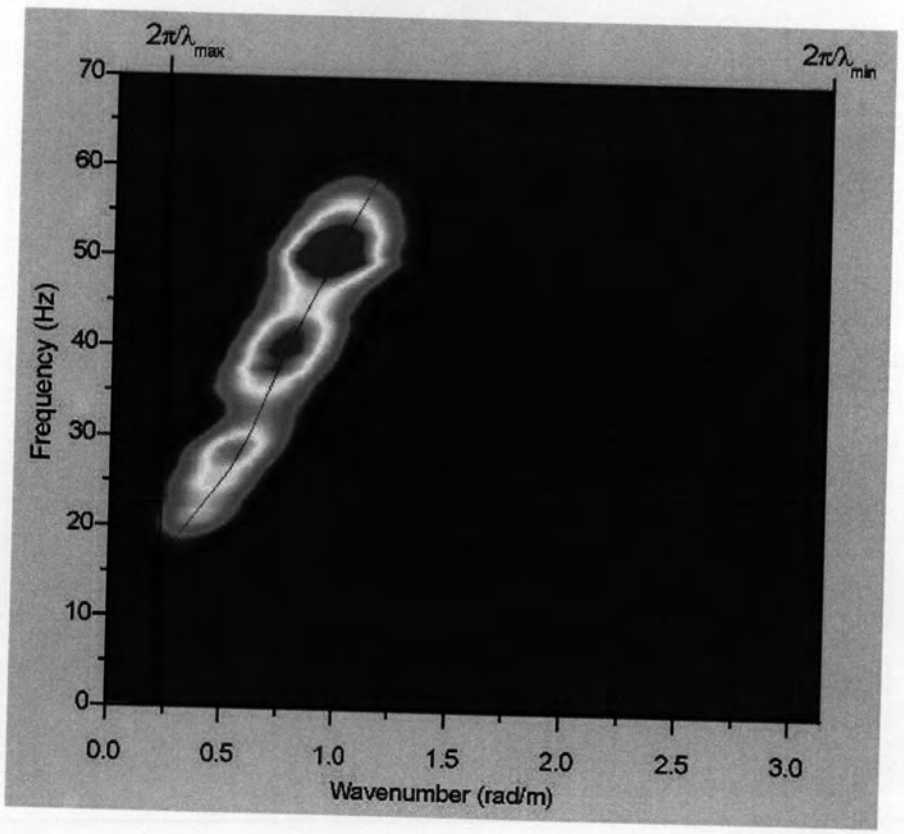

Figure 4-17 **Frequency wavenumber domain for Kirdkao Observatory, Kanchanaburi**

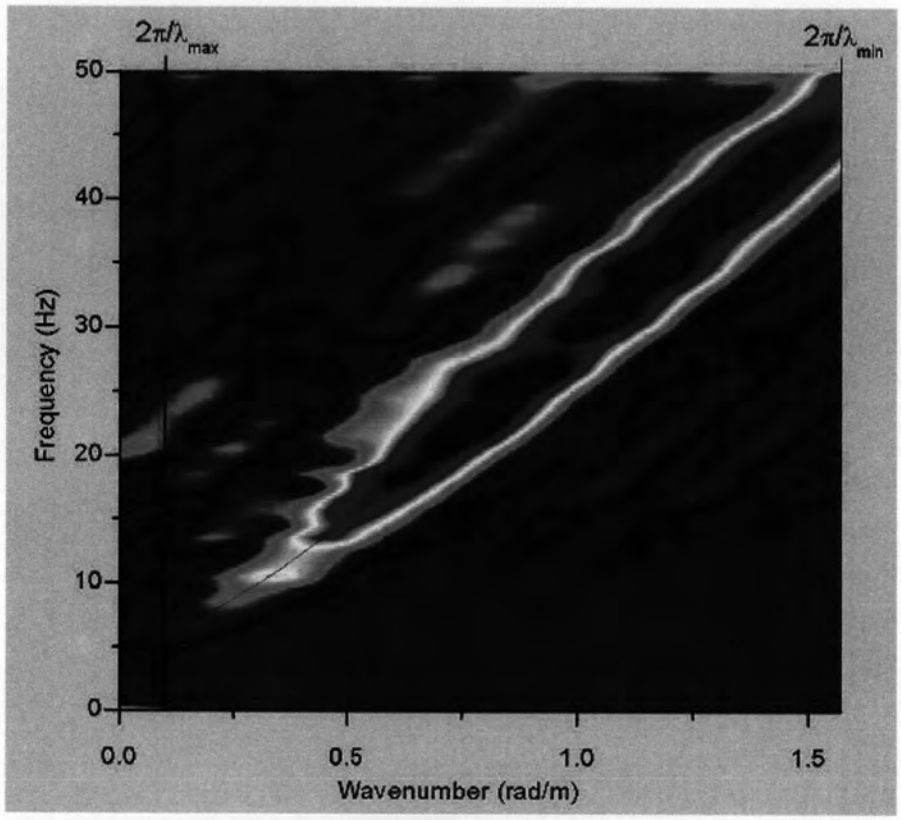

Figure 4-18 **Frequency wavenumber domain for TMD, Kanchanaburi**

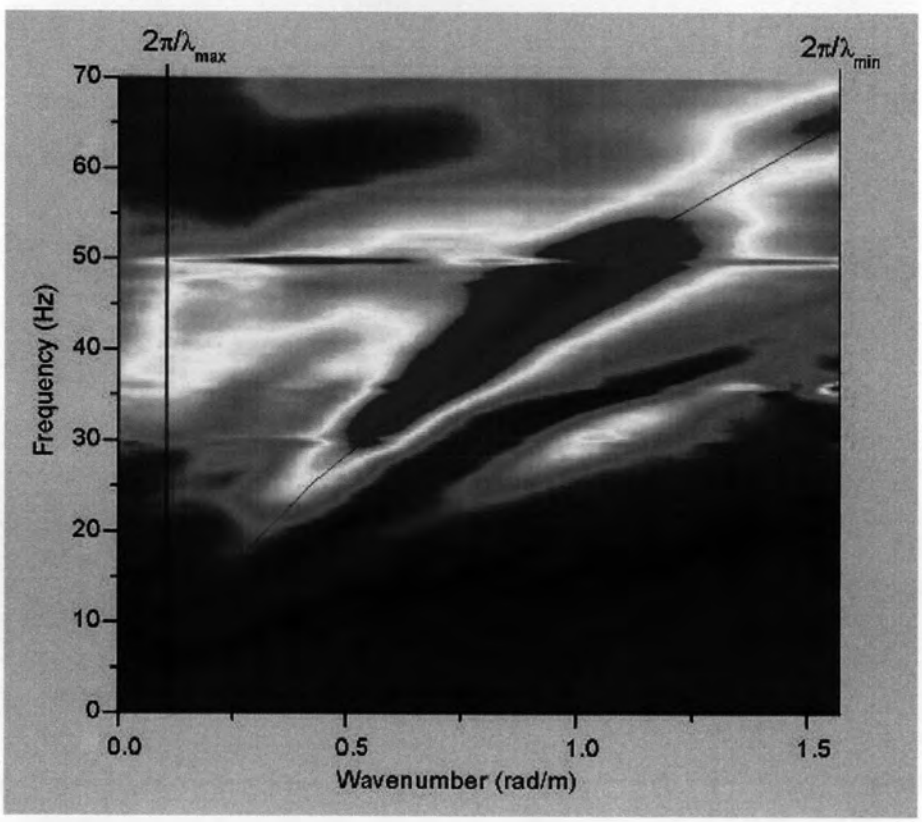

Figure 4-19 **Frequency wavenumber domain for Chiang Mai University**

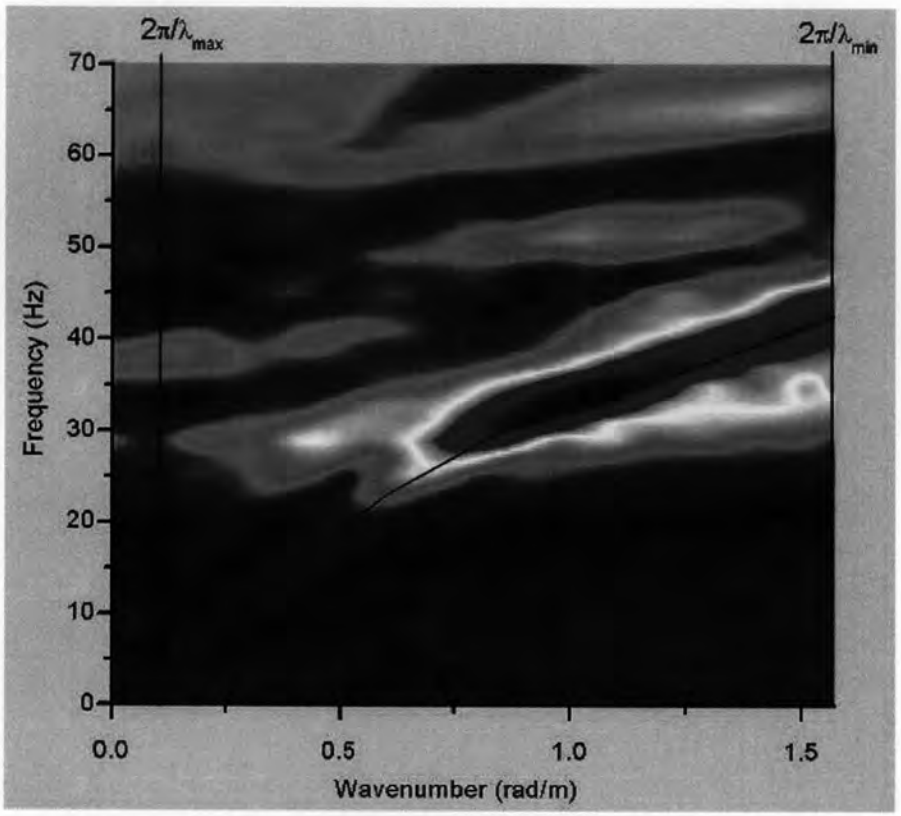

Figure 4-20 **Frequency wavenumber domain for Wat Chediluang, Chiang Mai**

Since the trace of peaks is corresponding to the ground roll, we will pick it for further analysis by drawing a polyline through that trace. The picked up coordinates are limited between $2\pi/\lambda_{max}$ to $2\pi/\lambda_{min}$ where values of the maximum and minimum wavelengths are determined by two times the largest and the smallest geophones spacing, respectively. The meaningful ranges in wavenumber and frequency domain are limited by Nyquist theory (equation 3.4 and 3.7), and are summarized in table 4-2:

Table 4-2 **the Nyquist frequencies and wavenumbers of seven sites**

Axes	a	b	c	d	e	f	g	Unit
f_{max}	500	500	500	500	500	500	500	Hz
k_{max}	0.79	1.57	1.05	3.14	1.57	1.57	1.57	Rad/m

Given that, the data set with function of frequency and wavenumber has a connection with frequency vs. phase velocity function through equation 3.2 and 3.3, the dispersion curves can be plotted as shown in figure 4-21 to 4-27.

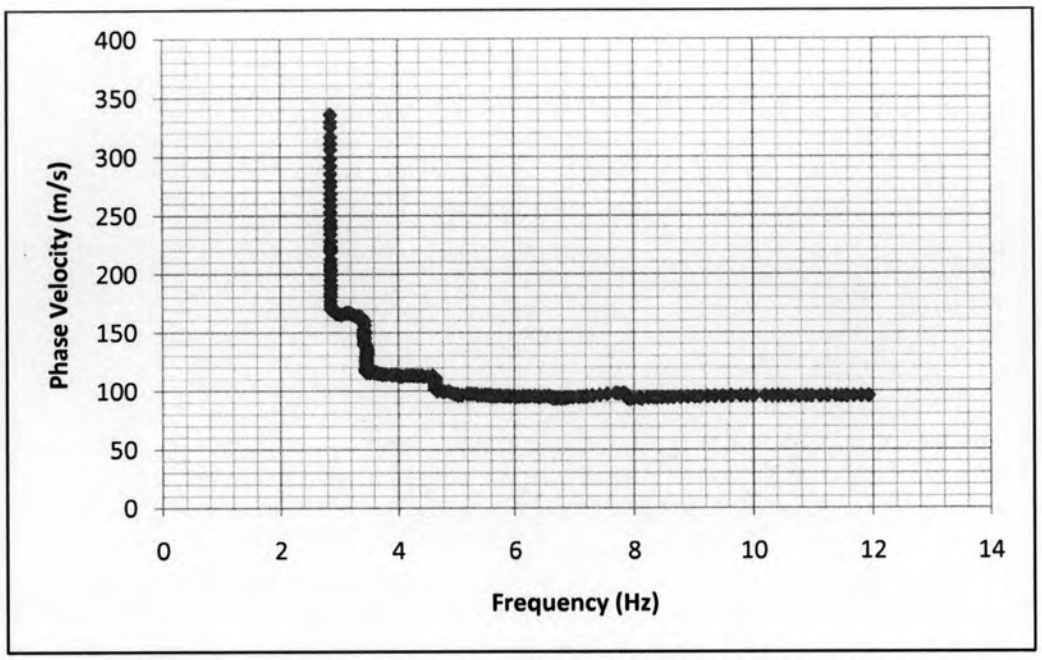

Figure 4-21 **The dispersion curve of subsoil at Chulalongkorn University**

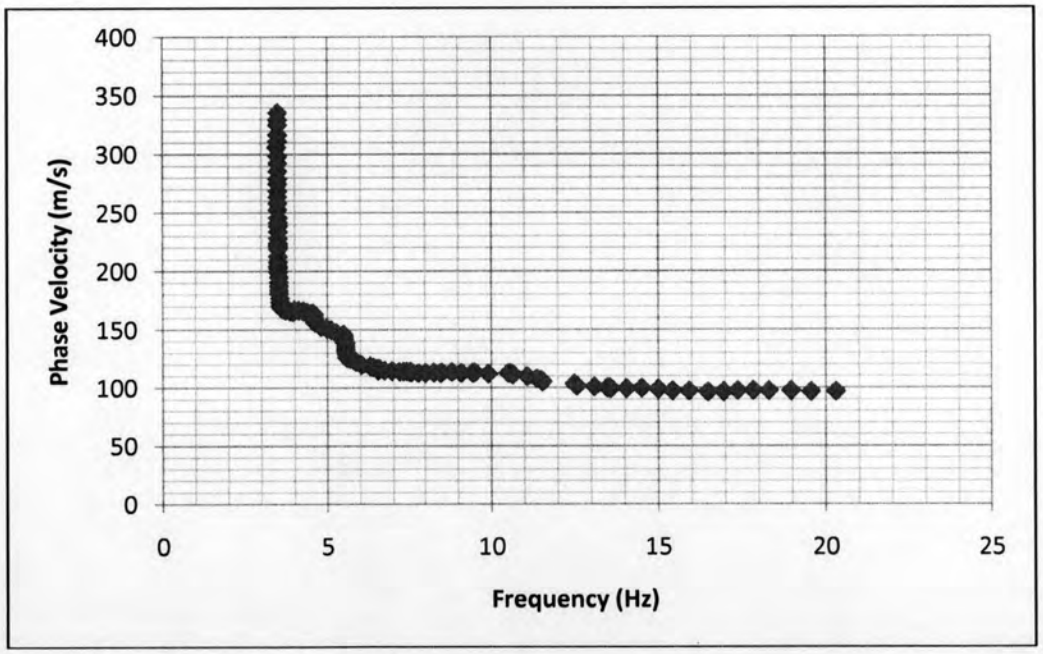

Figure 4-22 **The dispersion curve of subsoil at TMD Bangkok**

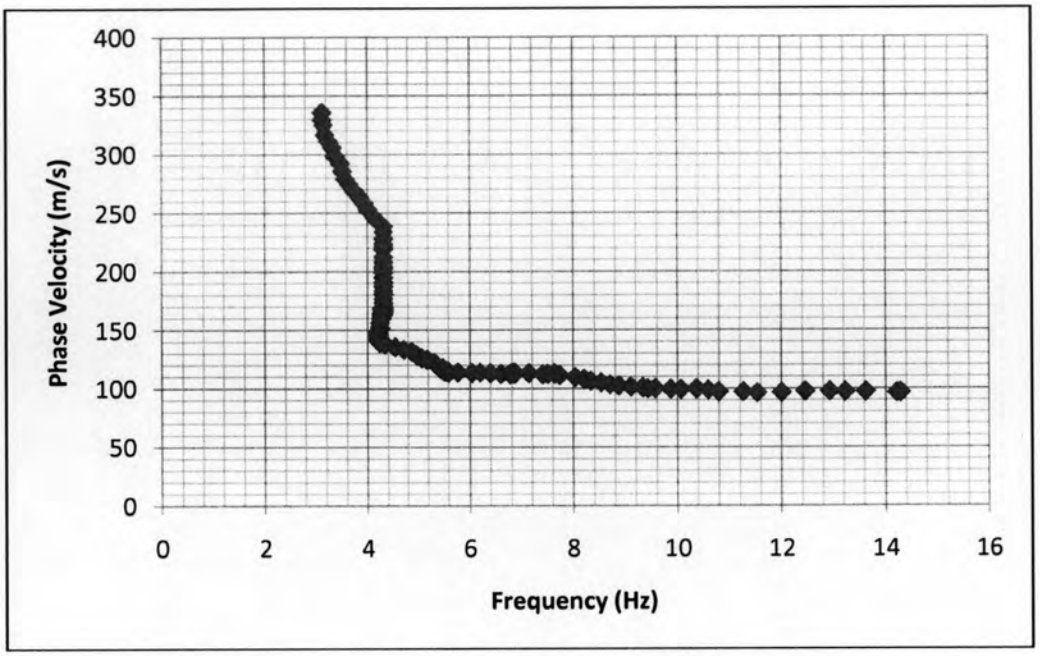

Figure 4-23 The dispersion curve of subsoil at AIT

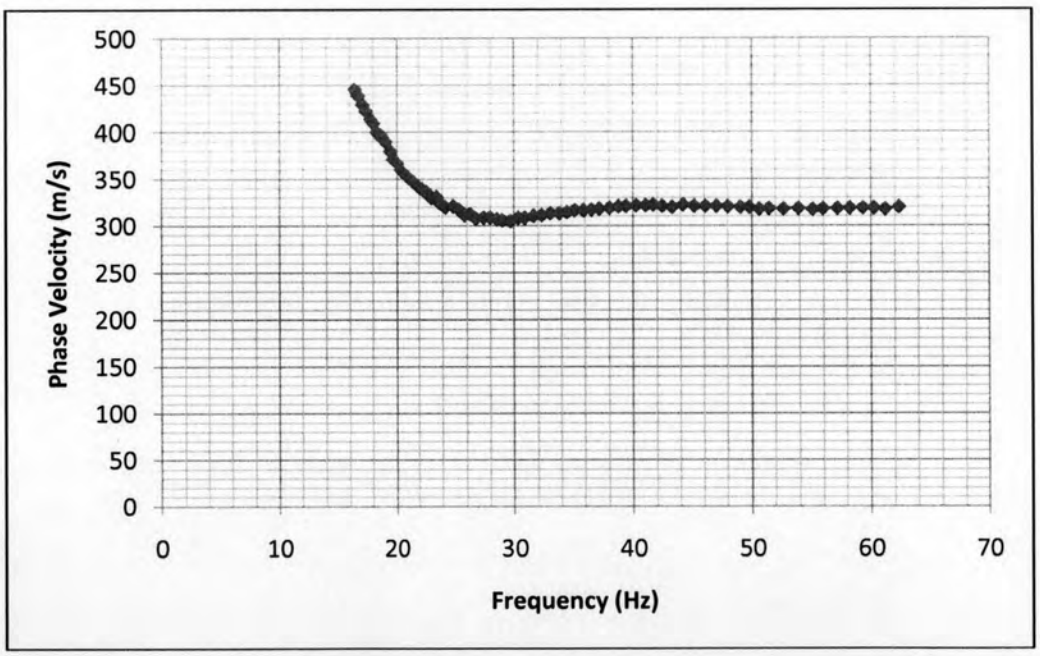

Figure 4-24 The dispersion curve of subsoil at Kirdkao Observatory, Kanchanaburi

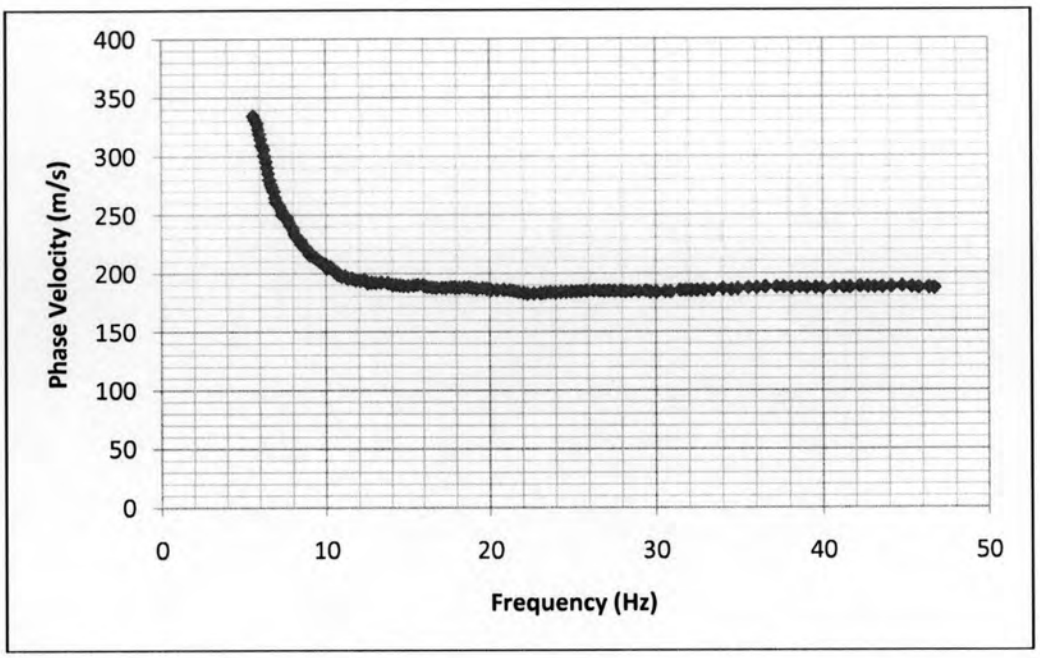

Figure 4-25 The dispersion curve of subsoil at TMD Kanchanaburi

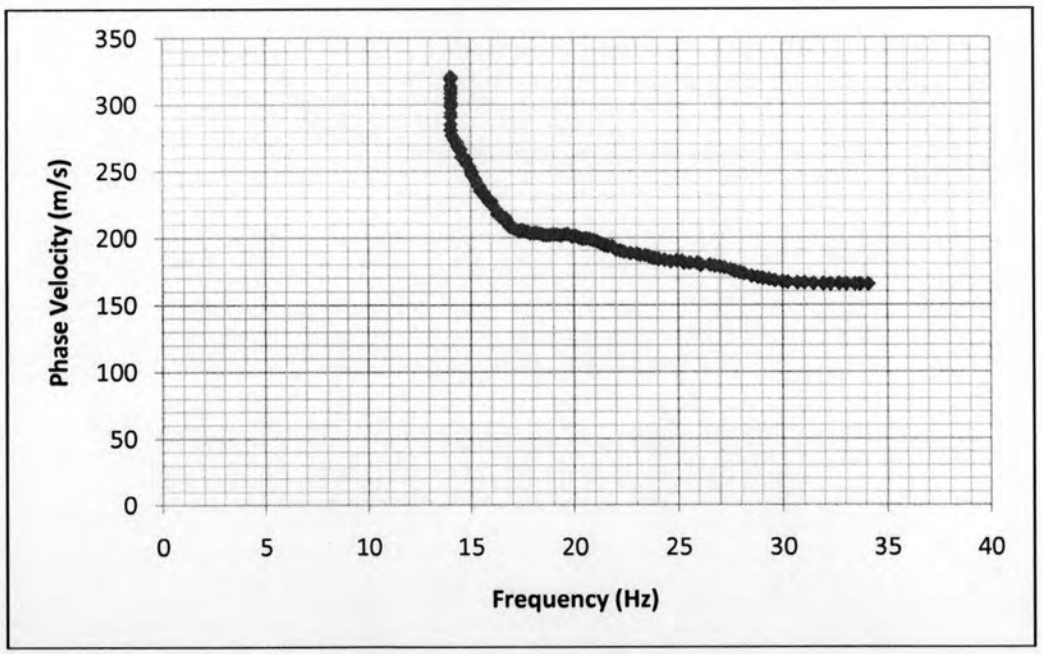

Figure 4-26 The dispersion curve of subsoil at Chiang Mai University

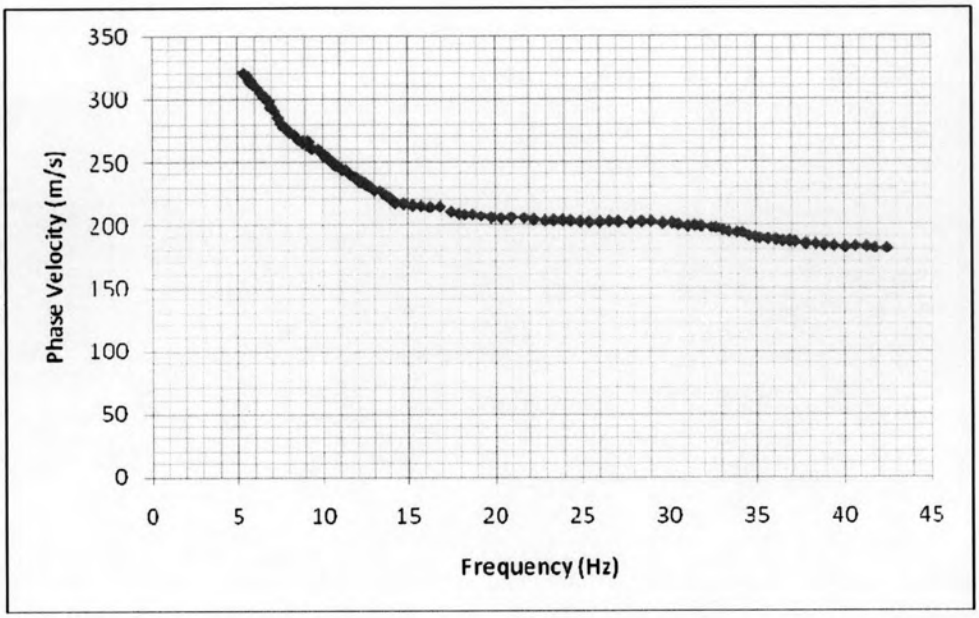

Figure 4-27 The dispersion curve of subsoil at Wat Chediluang, Chiang Mai

4.6 Data Inversion

The simplified inversion algorithm is then applied to the dispersion curve to attain the shear wave velocity profiles for each test. The algorithm is explained by the figure 4.28.

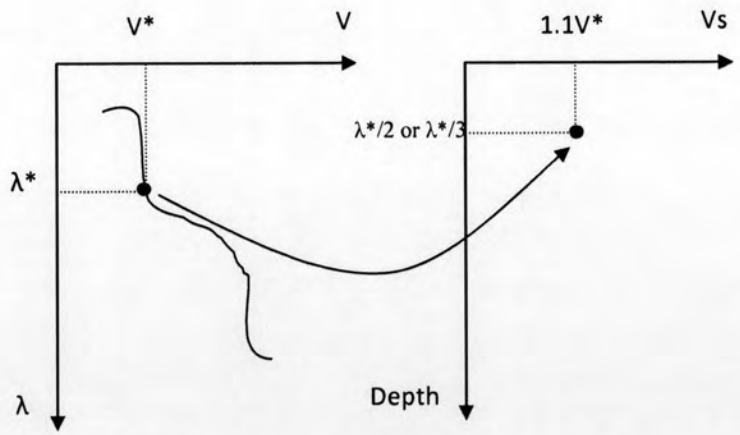

Figure 4-28 The simplified inversion process

Since we already had the dispersion curve of phase velocity as the function of frequency, we are also able to build it as the function of wavelength (λ-v)(figure 4-28), so that the inversion process is ready to proceed by equations (2.2 and 2.3). Consequently, Vs profiles are attained; two Vs profiles are computed from λ/2 and λ/3 algorithms for each site. The calculated Vs represents the profile at the middle of spread given that the signal from each geophone were automatically averaged by 2D FFT. The results are kept for later comparison with those from different kinds of test in the next chapter.